INSTITUTE OF PHYSICS PUBLISHING PLASMA SOURCES SCIENCE AND TECHNOLOGY
Plasma Sources Sci. Technol. **11** (2002) A138–A142 PII: S0963-0252(02)35514-2

Spatial distribution of turbulence in the Wendelstein 7-AS stellarator

N P Basse[1,2], P K Michelsen[1], S Zoletnik[3], M Saffman[4], M Endler[5] and M Hirsch[5]

[1] Association EURATOM—Risø National Laboratory, DK-4000 Roskilde, Denmark
[2] Ørsted Laboratory, Niels Bohr Institute for Astronomy, Physics and Geophysics, DK-2100 Copenhagen, Denmark
[3] CAT-SCIENCE Bt. Detrekő u. 1/b, H-1022 Budapest, Hungary
[4] Department of Physics, University of Wisconsin, Madison, WI 53706, USA
[5] Association EURATOM—Max-Planck-Institut für Plasmaphysik, D-85748 Garching, Germany

Received 29 September 2001, in final form 19 February 2001
Published 19 August 2002
Online at stacks.iop.org/PSST/11/A138

Abstract
In this paper measurements of short wavelength electron density fluctuations using collective scattering of infrared light are presented. The Wendelstein 7-AS (W7-AS) stellarator (Renner H *et al* 1989 *Plasma Phys. Control. Fusion* **31** 1579) and the diagnostic are briefly described. A series of plasma discharges with reproducible confinement transitions was created by ramping up the plasma current. Utilizing the fact that the density fluctuation wavenumber κ is anisotropic in the directions parallel and perpendicular to the local magnetic field, the diagnostic can provide a radial profile of the turbulence during both normal and degraded confinement. The found profiles display an increase of core turbulence for the reduced confinement state. The results are discussed and compared to similar tokamak measurements.

1. Introduction

The significant anomalous transport observed in toroidal fusion devices plays an important role in the global transport properties of plasmas [1]. Therefore, it is important that a continual effort is made to measure fluctuations in plasma parameters, since these are thought to be created by turbulent transport processes. The work presented here is measurements of fluctuations in the electron density of high temperature plasmas. The paper is organized as follows. In section 2 we describe the Wendelstein 7-AS (W7-AS) fusion machine and the experimental setup. In section 3, we present the discharges analysed. Section 4 contains a description of spatially localized measurements of fluctuations in the electron density of W7-AS plasmas using collective scattering of infrared light [2, 3] and a comparison of these to an empirical model of the spatial distribution of density fluctuations [4, 5]. Finally, in section 5 we relate the results to similar findings, both in W7-AS and the Tore Supra and DIII-D tokamaks.

2. W7-AS and the diagnostic

W7-AS is a modular stellarator of five-fold toroidal symmetry [6]. It has an average major radius $\langle R \rangle$ of 2 m, and an 'effective' radius $r_{\mathrm{eff}}(a)$ of maximum 18 cm (aspect ratio $\geqslant$11). The effective radius of a given magnetic flux surface is a convenient label (related to the actual radius of a torus that encloses the same volume as the chosen stellarator flux surface) that enables one to map the measurement positions of various diagnostics. The rotational transform ι can be altered between 0.27 and 0.7. The magnetic field structure varies as a function of the toroidal angle φ in W7-AS. To illustrate the complex field structure, figure 1 shows the flux surfaces (for an edge rotational transform ι_{a} of 0.344) at three toroidal positions. The dashed line displays the last closed flux surface (LCFS) defined by limiters.

The measurements of density fluctuations presented in section 4 were obtained using the LOcalized TUrbulence Scattering (LOTUS) diagnostic installed on W7-AS. For a detailed description of the diagnostic, see [7]. The setup is shown in figure 2. The main (M) continual wave 20 W CO_2 laser beam passes through a Bragg cell which creates a second local oscillator (LO) beam, i.e. frequency shifted 40 MHz with respect to the M beam (heterodyning). The two beams cross in the plasma, and their angle θ_{s} is proportional to the wavenumber $k_{\perp}$ of the observed density fluctuations. The measurement volume created by the crossed beams is

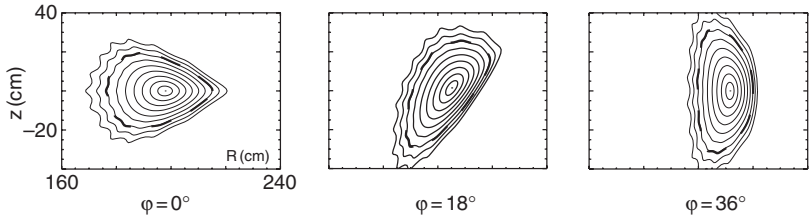

Figure 1. Flux surfaces at three toroidal angles φ: 0° is the triangular plane in the centre of a module, 18° is intermediate and 36° is where two modules meet. The corresponding negative angle flux surfaces are obtained by horizontal mirroring.

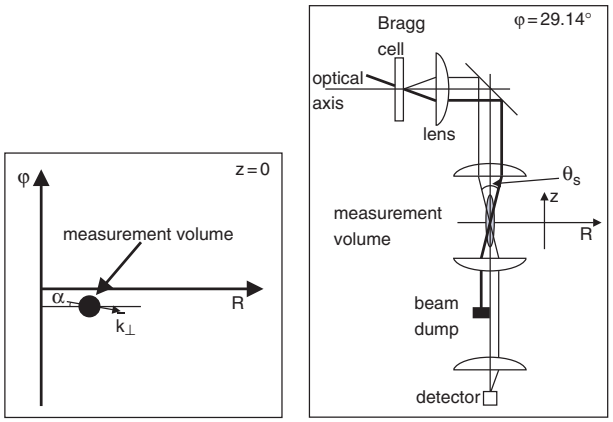

Figure 2. Left: view from above of the measurement volume created by two crossed beams having the same waist size; right: side view of diagnostic setup. The M beam is the thick line and the LO beam is the thin line.

vertical and passes through the plasma centre. We used a beam waist $w = 3.3\,\mathrm{cm}$ and measured fluctuations having $k_\perp = 15\,\mathrm{cm}^{-1}$ in the described experiments. The LOTUS diagnostic is positioned at $\varphi = 29.14^\circ$, which is close to the elliptical plane (see figure 1). The central equation describing the scattered power observed at the detector is

$$P(\alpha, k_\perp) \propto \int_{z_{\mathrm{bottom}}}^{z_{\mathrm{top}}} \delta n_{\mathrm{e}}^2(z) \exp\left(-\frac{1}{4}\left(\left[\alpha - \theta_{\mathrm{p}}(z)\right] w k_\perp\right)^2\right) \mathrm{d}z, \quad (1)$$

where α is the angle between the major radius R and $\bar{k}_\perp$ (see figure 2), δn_{e} is the RMS value of the electron density fluctuations and $\theta_{\mathrm{p}} = \arctan(B_R(z)/B_\varphi(z))$ is the horizontal pitch angle of the magnetic field [3]. Assuming that fluctuations parallel to the magnetic field (having wavenumber $\kappa_\parallel$) are very small compared to the fluctuations perpendicular to the field ($\kappa_\perp$) and knowing that θ_{p} changes 16° from the bottom to the top of our measurement volume, one can turn α and thereby effectively select a region in the plasma wherefrom the detected signal originates.

3. Discharge description

It is a well-known fact that slight changes in the ι_{a} of W7-AS discharges around major low-order rationals result in dramatic changes of the confinement. This phenomenon can be reproduced by an empirical model of the electron heat conductivity [8]. The confinement transition can be created in a dynamical fashion by ramping up the plasma current I_{p} during a discharge (see figure 3). Figure 3(*a*) shows the

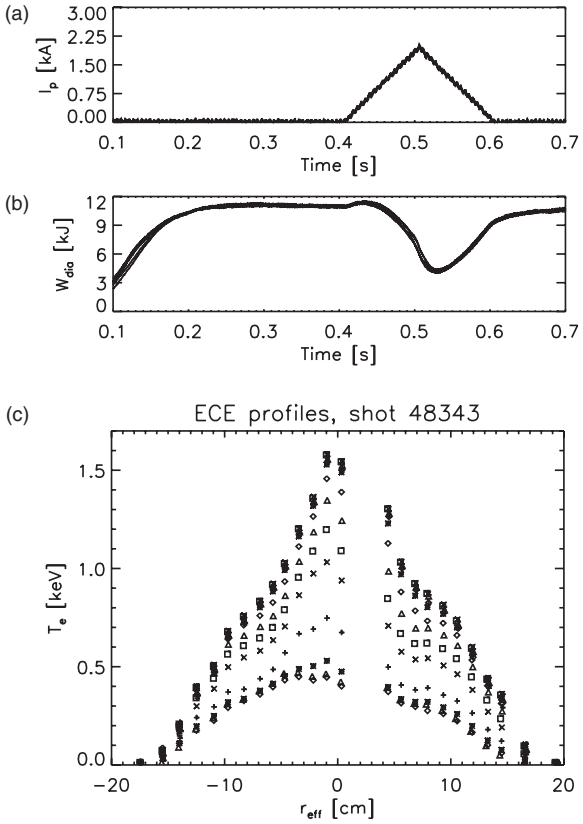

Figure 3. (*a*) Plasma current, (*b*) the diamagnetic stored energy and (*c*) ECE temperature profiles. The initial (high temperature) timepoint is marked by plusses, the following timepoints (10 ms apart) are represented by: asterisks, diamonds, triangles, squares and ×s (cyclic permutation of symbols).

plasma current as a function of time for six identical discharges. The current (mainly the bootstrap current in this case) was compensated to zero in the initial phase of the discharges using an external transformer. At 400 ms into the discharges, the current was ramped up to 2 kA in 100 ms and then ramped down again from 500 to 600 ms. The response in the stored energy of the plasma can be seen in figure 3(*b*): at about 250 ms into the shot, the plasmas have become stable in the low confinement (L) mode. The induced plasma current first leads to a small increase of confinement, thereafter the confinement degrades rapidly with a minimum at 530 ms. The lag of the confinement with respect to the current is due to the finite current penetration time into the plasma. As the current is ramped down again, the discharges recover to their pre-ramp confinement quality. The reason for the dramatic change of confinement is connected to modifications of the ι-profile

caused by the current ramping. A detailed analysis of these profiles is underway [9]. The main effect of the current ramp on the ι-profile is to increase ι in the core, thereby decreasing the shear and moving the ι-profile into a zone of rationals above $\iota = 1/3$. As the density profile was kept approximately constant during the confinement transitions by gas puffing, the change of stored energy was due to developments of the temperature profile. Figure 3(*c*) shows electron cyclotron emission (ECE) measurements of the electron temperature profiles during the transition from good (400 ms) to bad confinement (540 ms). The profiles are plotted 10 ms apart; in the good confinement phase the central temperature exceeds 1.5 keV, while the profile collapses during the transition to arrive at a central temperature of only 0.4 keV. The profile collapse appears to have two sequences: first, the temperature decrease is limited to the central plasma (400–480 ms); thereafter, also the edge gradient (transport barrier) collapses, leading to the final low 'sub-L-mode' confinement state [10]. The discharge parameters-at-a-glance were: deuterium plasma, 2.5 T field, 400 kW of ECRH heating, central electron density 8×10^{19} m^{-3} (the line density was kept constant by feedback gas puffing), central electron temperature 1.5/0.4 keV and stored energy 11/4 kJ for good/bad confinement, respectively.

4. Turbulence profiles

We now turn to the measurements. Six identical discharges were made (#48338-43), where we changed the diagnostic angle α between each shot. This is equivalent to a six-point turbulence profile. The measurement results are shown in figure 4. The curve connected by diamonds in the upper plot is frequency integrated scattered power during good confinement versus spatial position in normalized coordinates (-1 bottom LCFS, 0 centre, 1 top LCFS of plasma). The triangle curve shows the profile during bad confinement. Finally, the asterisk curve in the lower plot shows the bad/good profile ratio. The measurements were averaged over 50 ms, the good confinement data from 300 to 350 ms and the bad confinement ones from 500 to 550 ms. We can make the following statements: (1) the turbulence level is generally low in the central plasma as compared to the edge; (2) the turbulence level increases at all radial positions in going from good to bad confinement; (3) the increase in turbulence is largest in the central plasma; and (4) the ratio between bad/good profiles is shifted somewhat with respect to $r_{\rm eff}/r_{\rm eff}(a) = 0$. Item (4) indicates that our original α calibration is somewhat off with respect to the 'real' calibration.

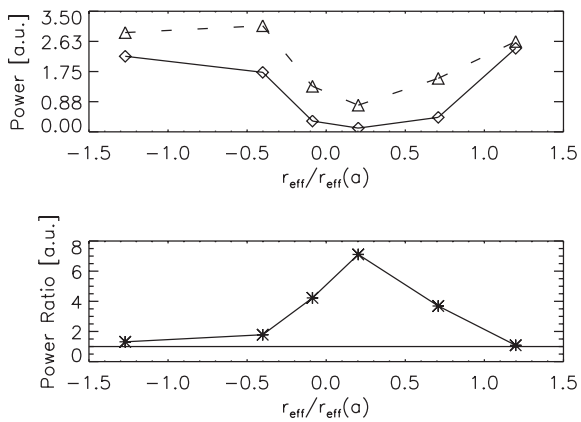

Figure 4. Measured turbulence profiles (top) and ratio between them (bottom). The symbols have the following meaning: diamonds (connected by ——) are good confinement, triangles (connected by · · · · · ·) bad confinement and asterisks the bad/good ratio.

At this point it is worth pointing out that our measurements are not direct measurements of the density fluctuation level; it is the fluctuation level multiplied by an instrumental function that constitutes our integrand in equation (1). However, by assuming that the 'real' fluctuation profile has certain properties, we can extract some information regarding the turbulence profiles.

We know all quantities entering the exponential factor in equation (1) and the measured scattered power P and will assume that the relative fluctuation level has the functional form

$$\frac{\delta n_{\rm e}(r_{\rm eff})}{n_{\rm e}(r_{\rm eff})} = b + c\left|\frac{r_{\rm eff}}{r_{\rm eff}(a)}\right|^{p}, \qquad (2)$$

where $n_{\rm e}$ is the electron density and (b, c, p) are fit parameters (see [4, 5] and references therein). The density profile used is obtained from Ruby laser Thomson scattering measurements. The task remaining is to perform a least-squares fit to the measured scattered power profiles in order to retrieve the relative fluctuation level. Since LOTUS is not absolutely calibrated, only relative levels can be obtained. The first step of the fit procedure was to re-calibrate α; this was done by making α into a fourth fit parameter and performing the fit. In fitting to all six points for both the good and bad confinement data, it was found that α increased for both cases, but not by the same amount. Excluding the spatial point 'pushed out' of the plasma in the direction indicated by the initial fits—and now only fitting to five points—the fitted α shifted by the same size in both cases, namely $1.65 \pm 0.03^{\circ}$ (of 16° in total, a change of 10%). The resulting positional change can be observed by comparing figures 4 and 5. In the fits described below, α was set to the re-calibrated value.

Unfortunately, this means that the bottom point of the profile can no longer be used in the fit since it is outside the plasma. The very limited number of measurement points of course questions the validity of the following procedure, since we use five data points to arrive at three fit parameters. However, this was the only series of similar discharges where we have data using the setup presented, and performing a least-squares fit is still the best way forward in the analysis of these discharges.

The result of the fits is shown in figure 5. The measured profile is displayed using the same symbols as in figure 4; squares are now the fit to good confinement and crosses fit to bad confinement. The errorbars on the measured data are set to 10%; for a treatment of the errors related to the diagnostic, see [11]. The fitted parameters were $(b, c, p)_{\rm good} = (0.0067, 0.53, 8.0)$ and $(b, c, p)_{\rm bad} = (0.019, 0.57, 6.2)$. Since we measure in arbitrary units, it is only the relative values $(c/b)_{\rm good} = 79$ and $(c/b)_{\rm bad} = 30$ that are important.

The relative $(\delta n_{\rm e}/n_{\rm e})$ and absolute $(\delta n_{\rm e}^2)$ fluctuation profiles are shown in figure 6. Note that the relative profiles are shown on a logarithmic plot to elucidate the core behaviour. The errorbars on the relative profiles are found using the

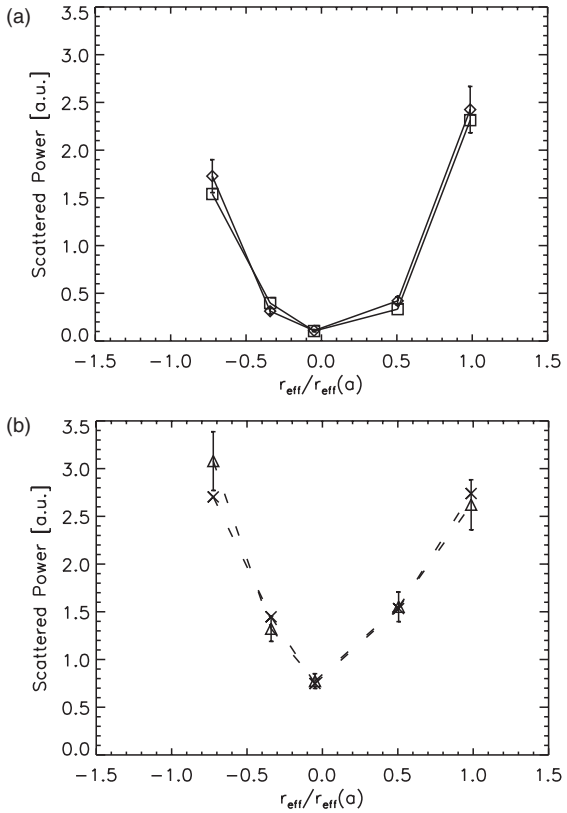

Figure 5. Measured and fitted profiles. (*a*) Good confinement (◇, □), (*b*) bad confinement (△, ×). The point beyond the bottom of the plasma is not included in the fits. The errorbars on the measured profiles are calculated assuming a 10% error.

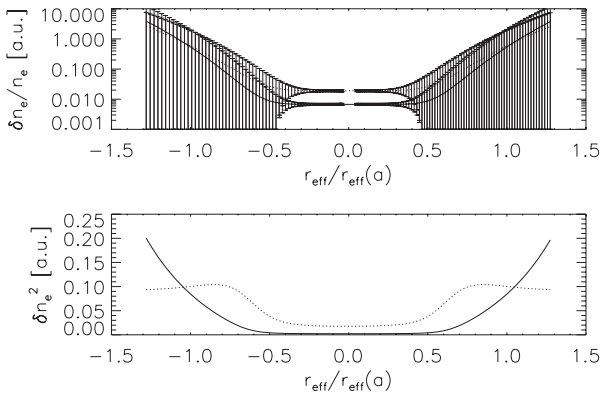

Figure 6. Fitted relative (top) and absolute (bottom) fluctuation profiles. Solid lines are good confinement, dotted lines are bad confinement profiles. Note that the data in the top plot are on a logarithmic scale. The errorbars on the relative profiles are calculated using the 10% error on the measured data.

covariance matrix obtained when applying the Levenberg–Marquardt method for the fit [12]. We conclude that the relative fluctuation level increases significantly in the core region of the plasma during degraded confinement. This is also the case for the absolute fluctuations, where the bad confinement profile furthermore develops a 'hump' somewhat inside the LCFS. The errorbars on the relative profiles show that the increased level of turbulence during bad confinement is a real effect. Outside half-radius, the profiles are identical within errorbars.

5. Discussion

We have in this paper presented an analysis where we arrived at density fluctuation profiles during two levels of confinement in the W7-AS stellarator. The procedure used is identical to the one used by the ALTAIR team at the Tore Supra tokamak to study differences between L-mode and reversed shear (RS) discharges [5, 13].

We have seen that the same model can be used in Tore Supra and W7-AS to fit the measured data; however, this is not surprising in our case, since our number of data points is very small compared to the number of fit parameters. Nevertheless, a direct comparison of L-mode parameters stated in [5] and derived above yields

$$\left(\frac{c}{b}\right)^{\text{W7-AS}}_{\text{L-mode}} = 79, \qquad p^{\text{W7-AS}}_{\text{L-mode}} = 8.0,$$
$$\left(\frac{c}{b}\right)^{\text{Tore Supra}}_{\text{L-mode}} = 14, \qquad p^{\text{Tore Supra}}_{\text{L-mode}} = 8.$$

From the above parameters it is quite difficult to make quantitative comparative remarks concerning the fluctuation profiles. Unfortunately, due to the installation of divertor modules in W7-AS (which severely limits the optical access), it is no longer possible to extend our measurement database.

A second point of some interest is that both the change from L-mode to RS confinement in Tore Supra and the sub-L- to L-mode transition in W7-AS is connected to a strong decrease of density fluctuations in the core plasma. A direct comparison of figure 6 in [5] and figure 6 (top) in this paper shows that the transition from bad to good confinement is mainly associated with a reduction of core turbulence.

Further evidence of the connection between reduced core turbulence (measured using beam emission spectroscopy) and improved plasma performance has been found in the DIII-D tokamak for both internal transport barrier and radiatively improved discharges [14].

The final point of our discussion concerns comparisons to measurements of density fluctuations in W7-AS using a Li-beam [15]. From this diagnostic one can obtain both the absolute and relative fluctuation level almost to the core for low densities. At higher densities, only information concerning the outer parts of the confined plasma and the scrape-off layer (outside the LCFS) can be measured. As is the case for the measurements presented above using the LOTUS diagnostic, measurements using the Li-beam have been made in discharges with current ramp induced confinement transitions.

It was found (see section III.C in [15]) that for low densities ($n_e = (1\text{–}2) \times 10^{19}\,\text{m}^{-3}$) the behaviour of the fluctuations changed in response to current ramping: the absolute level had a hump inside the LCFS without a current ramp, while this disappeared during the ramp; the relative fluctuation level also decreased during the ramp. However, the observed changes were not associated with any change of the global energy confinement. At higher densities (similar to the ones described in this paper), however, these changes in the fluctuations observed with the Li-beam did not take place, but a degradation of the confinement occurred (figure 3(*b*)).

These last observations seem in contrast to what we have found; with the LOTUS diagnostic, a significant change was indeed found in the turbulence behaviour between good and bad

confinement in high density discharges. However, the Li-beam only measures fluctuations from 80% of the plasma radius and outward at these densities, which is a region where we have seen that the fluctuation level is roughly unchanged (figure 6).

References

[1] Liewer P C 1985 *Nucl. Fusion* **25** 543
Wootton A J *et al* 1990 *Phys. Fluids* B **2** 2879
Carreras B A 1997 *IEEE Trans. Plasma Sci.* **25** 1281

[2] Surko C M *et al* 1976 *Phys. Rev. Lett.* 1747
Holzhauer E *et al* 1978 *Plasma Phys.* **20** 867
Slusher R E *et al* 1980 *Phys. Fluids* **23** 472

[3] Truc A *et al* 1992 *Rev. Sci. Instrum.* **63** 3716

[4] Devynck P *et al* 1993 *Plasma Phys. Control. Fusion* **35** 63

[5] Antar G *et al* 2001 *Phys. Plasmas* **8** 186

[6] Renner H *et al* 1989 *Plasma Phys. Control. Fusion* **31** 1579
Jaenicke R *et al* 2000 *Proc. 18th IAEA Fusion Energy Conf. IAEA-FI-CN-77/OV4/3 (Sorrento, Italy)*

[7] Saffman M *et al* 2001 *Rev. Sci. Instrum.* **72** 2579

[8] Brakel R *et al* 1997 *Plasma Phys. Control. Fusion* **39** B273
Brakel R *et al* 1998 *25th EPS Conf. on Controlled Fusion and Plasma Physics (Prague)* Europhysics Conference Abstracts **22C** 423

[9] Zoletnik S *et al* 2002 *Plasma Phys. Control. Fusion* **44** in press

[10] Wagner F *et al* 1998 *Proc. 17th IAEA Fusion Energy Conf. IAEA-FI-CN-69/OV2/4 (Yokohama, Japan)*

[11] Basse N P 2002 *PhD Thesis* University of Copenhagen

[12] Press W H *et al* 1994 *Numerical Recipes in Fortran* (Cambridge: Cambridge University Press)

[13] Hoang G T *et al* 2000 *Phys. Rev. Lett.* **84** 4593

[14] Greenfield C M *et al* 1999 *Nucl. Fusion* **39** 1723
McKee G R *et al* 2000 *Phys. Plasmas* **7** 1870

[15] Zoletnik S *et al* 1999 *Phys. Plasmas* **6** 4239